The heart of oxygenic photosynthesis illuminated

Janssen, G.J.

Chapter 1

INTRODUCTION

1.1 OXYGENIC PHOTOSYNTHESIS

1.1.1 Solar energy

Over the past 3.5 billion years, nature has developed a highly efficient mechanism to harvest solar energy resulting in the process we now know as photosynthesis (Blankenship 2002). Today photosynthesis is crucial for life on earth just as energy is crucial to maintain our current state of human civilization. Besides the production of oxygen, photosynthetic processes lead to the formation of fossil fuels. In addition, photosynthetic organisms are the start of the food chain and as such sustain living beings on the planet.

The capability to harvest energy from sunlight by 'soft' biological proteins has triggered an extensive amount of research. By increasing our understanding about photosynthesis, we ultimately aim to find sustainable solutions for man's increasing demand for energy while avoiding both the excessive use of fossil fuels that cause environmental problems and the danger involved with nuclear power plants. The accident at the nuclear power plant of Fukushima in Japan 2011 underlined once again the necessity to find a safe and green alternative source of energy (Knip 2011).

1.1.2 Photosynthetic proteins

The primary photosynthetic processes of energy conversion occur inside the reaction center (RC), a pigment-protein complex located at the heart of the photosynthetic complexes. Upon the absorption of a photon in the visible region, a cascade of electron transfer reactions occurs along a series of protein-bound cofactors, leading to the formation of a trans-membrane potential. There are two types of RCs distinguished based upon their final electron acceptor: Type I RCs have iron-sulfur clusters as electron acceptors while Type II RCs contain pheophytin and quinone as acceptors. Photosynthetic purple bacteria and green non-sulphur bacteria have Type II RCs while Type I RCs are found in heliobacteria and green sulphur bacteria.

Photosynthesis in cyanobacteria, algae and higher plants involves the participation of both types of RCs, photosystem I (PSI, Type I) and photosystem II (PSII,

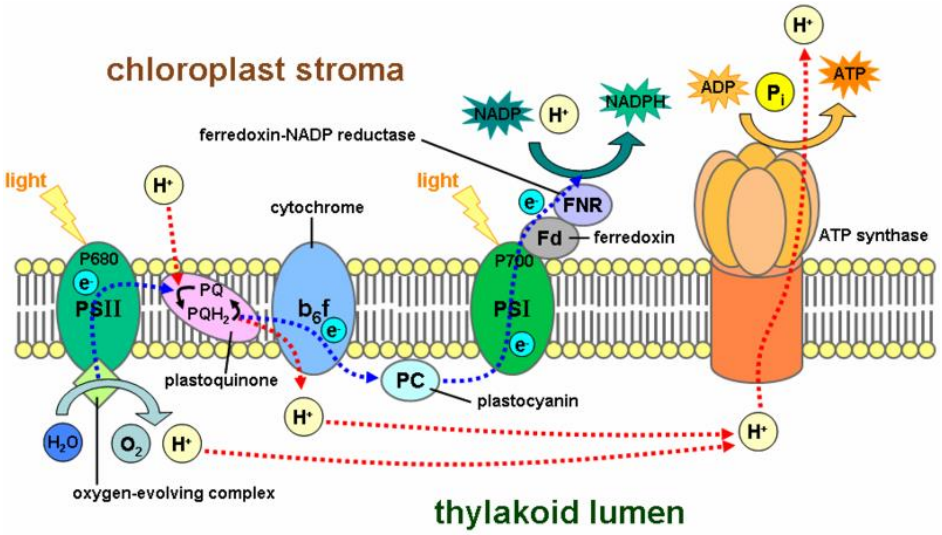

Figure 1.1: Schematic model of the photosynthetic machinery of oxygenic photosynthesis as found in plants, green algae and cyanobacteria located in the thylakoid membrane. Electron transfer starts at photosystem II (PSII) and proceeds via the plastoquinone pool to cytochrome b_6f and via plastocyanin to photosystem I (PSI). The proton gradient that is generated drives the synthesis of ATP by the ATP synthase complex. The electron transport chain is depicted in blue dotted arrows; the proton transport chain is depicted in red dotted arrows.

Type II). The coupling of these two photosystems allows for the pumping of electrons across the photosynthetic membrane, transforming the energy from the sun into a stable trans-membrane potential that is strong enough to split water and reduce $NADP^+$. During this process, which is known as oxygenic photosynthesis, free oxygen is produced as a side product while carbon dioxide is fixed from the air into organic material. Figure 1.1 shows a schematic representation of the complexes involved in oxygenic photosynthesis and the proton and electron flows. The photosynthetic complexes are embedded inside the thylakoid membrane and while electrons are transferred from PSII to PSI, protons are pumped from the stroma (outer) to the lumen (inner) site of the thylakoid membrane. The potential difference generated by this movement is used to generate ATP. The active site of PSII, where water splitting occurs, protrudes into the acidic (pH 6.5) lumen space of the membrane while PSI functions at the stroma side where the pH is normally around 8 (Magnitskii and Tikhonov 1998; Kramer *et al.* 1999; Trubitsin and Tikhonov 2003). In plants and algae the thylakoid is located in specialized organelles called chloroplasts, with each cell containing 10 to 100 chloroplasts (Allen *et al.* 2011). Cyanobacteria are single cell organisms without separate chloroplasts, instead they contain a network of circular thylakoid membranes (Nowaczyk *et al.* 2010).

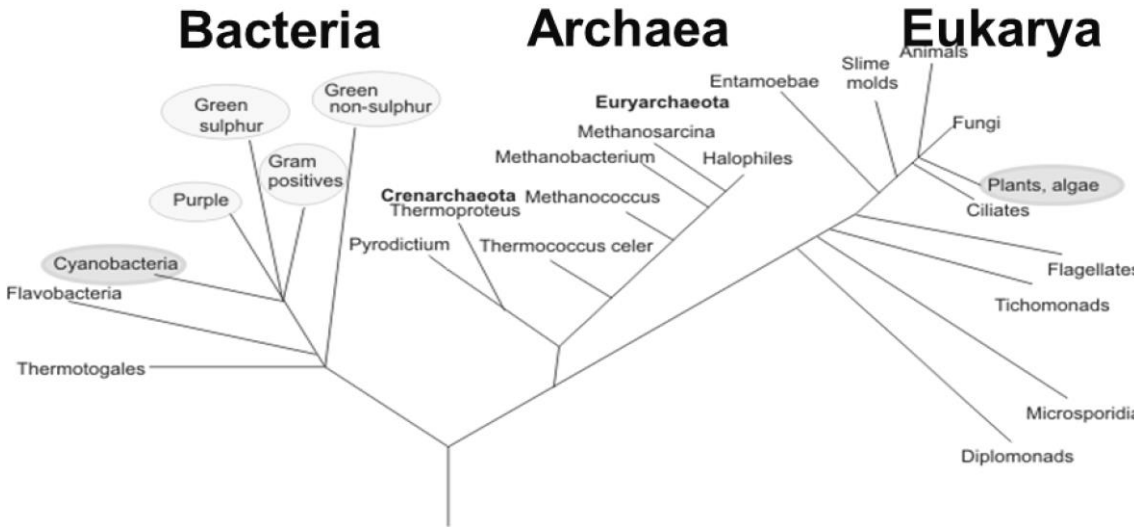

Figure 1.2: Phylogenetic tree based on the small subunit RNA method with the groups containing photosynthetic organisms marked by the grey circles (Blankenship 2002). Groups containing the full oxygenic photosynthesis machinery (PSI and PSII) are dark grey encircled. In bright grey are the groups that contain non-oxygenic photosynthetic organisms with either Type I or Type II photosystems.

1.1.3 Bacterial Reaction Centers

Figure 1.2 shows a phylogenetic tree indicating the groups that contain photosynthetic organisms (Blankenship 2002; Jankowiak *et al.* 2003). Although the occurrence of photosynthesis is widespread among distinct groups and different species, the overall three-dimensional structure of the photochemically active RC is highly conserved. In 1988 Deisenhofer, Michel and Huber shared the Nobel Prize in chemistry. They received the award for the determination of the first crystal structure of the RC of the purple bacteria *Rb. sphaeroides* (Deisenhofer *et al.* 1984; 1985), which was also the first resolved membrane protein complex. Because until the mid 80's this remained the only RC from which a high resolution X-ray structure was available, the Type II bacterial reaction center of purple bacteria is the most extensively studied photosynthetic RC (Hunter *et al.* 2008). The understanding of its function and structure has been used as a guideline for further research on other photosynthetic RCs.

Figure 1.3 shows the photosynthetic RC complex and the cofactor arrangement of the Type II bacterial reaction center of *Rb. sphaeroides* based on the 2.55 Å resolution X-ray structure solved by Camara-Artigas *et. al.* (Camara-Artigas *et al.* 2002). The RC consists of three membrane spanning polypeptides, L, M and H, referring to their relative (light, medium and heavy) weight (Yeates *et al.* 1987; Ermler *et al.* 1994; Camara-Artigas *et al.* 2002). The L and M proteins bind the cofactors. Two bacteriochlorophyll *a* (BChl *a*)

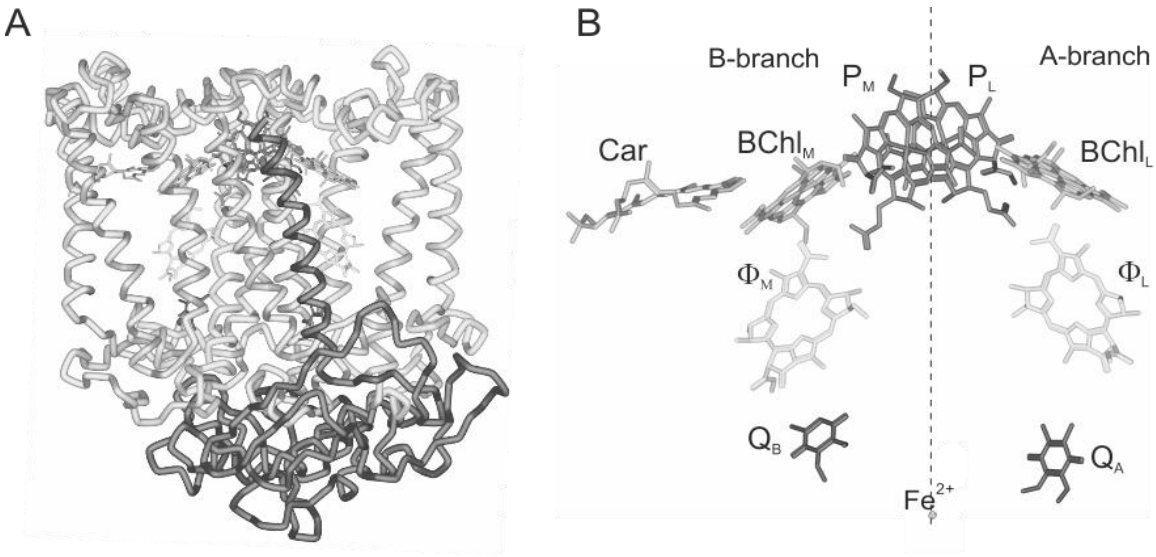

Figure 1.3: (A) The complex arrangement of 3 polypeptide subunits, L, M and H, that surround the bacterial RC are represented with a ribbon representation. (B) The cofactors in the bacterial reaction center (RC) of *Rb. sphaeroides* wild type (WT). The primary electron donor, the special pair, is formed by the two BChl *a* molecules P_L and P_M. $BChl_L$ and $BChl_M$ are accessory BChl cofactors. Φ_A and Φ_B are bacteriopheophytin (BPhe) *a* cofactors. On the acceptor side, two ubiquinone-10 cofactors Q_A and Q_B with a non-heme iron in between are localized. Side chains are omitted for clarity of representation. The near symmetric cofactor arrangement is broken by a carotenoid (Car). The light-induced electron transfer occurs selectively via branch A. [PDB entry 1M3X (Camara-Artigas *et al.* 2002), the figure has been made with Accelrys Discovery Studio adapted with permission from (Gupta 2011), page 17]

P_L and P_M form together the 'special pair' (P) or P840 donor. Although they are strongly coupled, P_L and P_M are not a perfect symmetric dimer (Hoff and Amesz 1991) and are therefore referred to as the 'special pair' rather than a BChl dimer. In addition two accessory BChl's ($BChl_{L,M}$), and two bacterial pheophytins ($\Phi_{L,M}$) are bound, with the subscripts representing the respective polypeptide chain to which the cofactor is bound (Deisenhofer *et al.* 1984). The Type II bacterial RC contains two ubiquinone-10 cofactors; Q_A and Q_B, with Q_B being more loosely bound and functioning as a two electron shuttle by dissociating from the RC after take up of two electrons and two protons. In addition the bacterial RC contains one spheroidene carotenoid (Car) and a non-heme iron (Fe^{2+}). The cofactors are arranged in two branches, A and B, around a pseudo-C_2 symmetry axis perpendicular to the membrane plane. The electron flow is asymmetric, occurring almost exclusively along the active A branch.

The carotenoid that is bound to the M subunit and located on the inactive branch near the $BChl_M$, breaks the apparent symmetry of the cofactor arrangement. Carotenoids are known to play an important role as light-harvesting pigments and in the prevention of the photochemical formation of highly reactive singlet oxygen species (Cogdell *et al.* 2000). Singlet oxygen is an extremely damaging species produced for example via the

triplet state of a Chl. The triplet Chl can be quenched by carotenes according to the Dexter triplet quenching mechanism (Dexter 1953; Cogdell *et al.* 2000), producing triplet Car (^{3}Car) that decays to the ground state by dissipating heat through molecular vibrations (Telfer 2005). The Dexter mechanism requires an electronic exchange coupling of the (BChl) donor and acceptor (Car) through an overlap of the respective wave functions. This mechanism is only efficient when donor and acceptor are in van der Waals contact. In the bacterial RC this condition is met with a distance between the $BChl_M$ and the Car of ~3.3 Å (Camara-Artigas *et al.* 2002). The *Rb. sphaeroides* R26 strain (R26) is a widely studied mutant that lacks the carotenoid. It has been found that after Car reconstitution into the R26 RC, two stereoisomers (13,14 -cis and 15,15'-cis) of the Car occur (Wirtz *et al.* 2007; Mathies *et al.* 2011). Recently however it has been shown by resonance Raman and DFT calculations that in the RC of *Rb. sphaeroides* WT the Car is in a 15,15'-cis configuration (Mathies *et al.* 2011). A quantitative comparison of the yields of triplet formation in wild-type (WT) and R26 with reconstituted Car is yet to be performed. This could give information on how critical the 15,15'-cis configuration of the Car is and thereby on the triplet quenching mechanism.

Solid state photo-CIDNP NMR studies have shown that the asymmetric ET in the bacterial RC is supported by symmetry breaking in the electronic groundstate (Schulten *et al.* 2002; Prakash *et al.* 2007; Alia *et al.* 2009). Although the exact origin has remained unclear, electrostatic interactions within the BChl *a* of the special pair, and conformational tuning of the cofactors by the protein environment are suggested to play an important role in determining the structure and electronic distribution of the special pair (Alia *et al.* 2009; Daviso *et al.* 2009; Ganapathy *et al.* 2009). ^{1}H-^{13}C heteronuclear dipolar correlation studies on [$^{13}C_6$,$^{15}N_3$]-His-labeled bacterial RCs and DFT calculations, indicated that especially the differential charge polarization of the axial histidine, His-L173, which is coordinated to the Mg^{2+} of the P_L BChl *a* cofactor, balances the asymmetry of the special pair for the bacterial RC in its groundstate (Alia *et al.* 2009).

1.1.4 Photosystem II

The PSII complex, which is depicted in Figure 1.4A, is the only protein complex capable of oxidative water splitting. Its biophysical processes have been the subject of many studies using a wide variety of techniques including: spectral hole-burning (Tang *et*

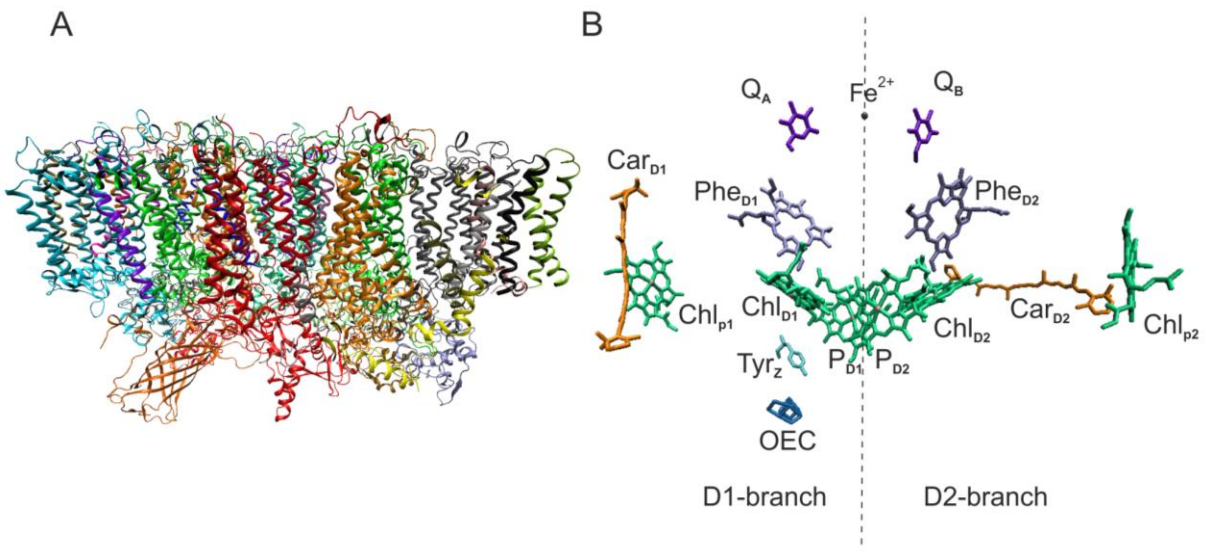

Figure 1.4: (A) The complex arrangement of homodimeric PSII with the polypeptide subunits represented in different colors with a ribbon representation. The D1 and D2 polypeptide subunits surrounding the PSII RC are depicted in orange and green, respectively. (B) The arrangement of cofactors in the PSII RC. The PSII RC consists of two central Chls (P_{D1} and P_{D2}), two accessory Chl *a* (Chl_{D1} and Chl_{D2}), two pheophytins (Phe_{D1} and Phe_{D2}), two Quinone's (Q_A and Q_B), and two peripheral Chl a (Chl_{p1} and Chl_{p2}) The cofactors are arranged in two symmetric branches, an active D1 branch (left) and an inactive D2 branch (right). Two β-carotenoids (Car_{D2} and Car_{D1}) are associated with the PSII core complex. At the P_{D1} donor side a Tyrosine residue Tyr_Z is bridging in ET between the P_{D1} and the Oxygen evolving complex (OEC). [PDB entry 3ARC (Umena *et al.* 2011)]

al. 1990; Tang *et al.* 1991; Jankowiak *et al.* 2003; Zazubovich *et al.* 2003; Riley *et al.* 2004), stark spectroscopy (Frese *et al.* 2003), photon echo (Prokhorenko and Holzwarth 2000), time-resolved-fluorescence (Novoderezhkin *et al.* 2005), visible pump-probe (Groot *et al.* 1997), 2D spectroscopy (Myers *et al.* 2010), photo-CIDNP (Matysik 2000; Diller *et al.* 2005; Diller *et al.* 2007; Diller *et al.* 2007), mutagenesis studies (Alizadeh *et al.* 1995; Diner *et al.* 2001; Wang *et al.* 2002; Schlodder *et al.* 2008) and theoretical calculations (Raszewski *et al.* 2005; Novoderezhkin *et al.* 2007; Raszewski *et al.* 2008; Kitagawa *et al.* 2011). PSII is a multiprotein complex found in higher plants, algae and cyanobacteria. Recently a high resolution X-ray structure of a dimeric PSII core complex from cyanobacteria *Thermococcus vulcanus* has been solved (Umena *et al.* 2011). Based on the available X-ray structures PSII was believed to function predominantly as a homodimer *in vivo*, but recent studies suggested that cyanobacteria might contain monomeric PSII (Zouni *et al.* 2001; Kamiya and Shen 2003; Biesiadka *et al.* 2004; Loll *et al.* 2005). The entire homodimeric PSII supercomplex consists of about 20 subunits, but variations are possible between PSII from different organisms. The PSII monomeric 'core complex' (~350 kDa) includes the PSII RC with the associated RC cofactors and a total of

12 β-carotenes. In addition the PSII core contains two integral antennae proteins CP43 and CP47, the α and β subunits of the cytochrome b559 complex (Cytb559), and a variable number of extrinsic proteins needed for the stabilization of the oxygen evolving complex (OEC) (Bricker *et al.* 2012).

The OEC is the water-oxidizing enzyme which catalyses the splitting of water and is bound to residues of the D1 protein and the integral antennae protein CP43. The OEC core consists of a cluster of four manganese ions, a calcium ion and five oxygens (Mn_4CaO_5), and is surrounded by amino acid chains. It is generally accepted that the OEC can exist in 5 states; S0 to S4, as was first described in 1970 by the Kok model (Kok *et al.* 1970). Many attempts to copy the catalytic power of the OEC by a stable artificial system have been made by either molecular mimicking of the OEC structural and functional features or by constructing artificial photocatalytic systems based on inorganic semiconductor materials and modular molecular assemblies (Boghossian *et al.* 2011; Li and Fan 2011). However, a truly biomimetic catalytic system that matches the performance of photosystem-II for efficient water splitting, operating with four consecutive proton coupled electron transfer steps to generate oxygen and hydrogen for hundred thousands of cycles at high rate is yet to be achieved. Recently a robust mono-iridium complex was presented for electrocatalytic water splitting (Joya *et al.* 2012). This iridium complex had a catalytic turn over number of more than 210 000 and an oxygen generation current densities of over 1.70 mA cm^{-2}. This is an example of a complex that could help to pave the way for photoelectrocatalytic devices with immobilized mono-site molecular complexes for future fuel generation from water splitting.

1.1.4.1 The Photosystem II RC

The PSII RC was first isolated in 1987 by Nanba and Satoh (Nanba and Satoh 1987). Figure 1.4B shows the arrangement of the cofactors inside the PSII RC which, in contrast to the several differences in the composition of the minor subunits of the PSII supercomplex, is highly conserved among different species. The reaction center contains two inner Chl *a* molecules (P_{D1} and P_{D2}, together denoted as P680), two accessory Chls (Chl_{D1} and Chl_{D2}, two pheophytins (Phe_{D1} and Phe_{D2}) and two quinones (Q_A and Q_B) bound to the D1 and D2 polypeptides. The arrangement of the cofactors inside PSII is similar to that known from RCs of purple bacteria, and the high resolution X-ray data

confirmed a homology between the amino acid sequences of the D1 and D2 subunits and their bacterial counterparts L and M (Deisenhofer *et al.* 1985). The P_{D1} and P_{D2} chlorophylls are the structural analogues of P_L and P_M, while the Chl_{D1} and Chl_{D2} and Phe_{D1} and Phe_{D2} correspond to respectively the $BChl_{L,M}$ and $\Phi_{L,M}$ cofactors in bacterial RC.

Two carotenoids, β-carotenes, are associated to the PSII RC with the Car_{D1} at a distance of ~20 Å from the Chl_{D1}, while Car_{D2} is ~13.2 Å away from Chl_{D2} (Loll *et al.* 2005). The bacterial RC on the other hand, contains one spheroidene Car, located within van der Waals distance, d_{vdW} ~3.6 Å, from the accessory $BChl_M$ (Camara-Artigas *et al.* 2002). In the PSII RC the Car cannot be in close proximity to the Chls, since the Car would be oxidized as a consequence of the high redox potential of PSII (Tracewell *et al.* 2011). Hence, efficient Chl triplet quenching by the Dexter mechanism, as is observed in the bacterial RC, is not possible for PSII. The Car in PSII do scavenge singlet oxygen species and transfer electrons to the $P680^{\bullet+}$ in case of over-reduction on the acceptor side (Hanley *et al.* 1999). In the antennae carotenoids protect against over-excitation in a range of mechanisms called "non-photochemical quenching" (NPQ) (Holt *et al.* 2004). Besides their photo-protective role, carotenoids in PSII are essential for the assembly of the D1 and D2 (Herrin *et al.* 1992) and function as light harvesting pigments (Frank and Cogdell 1996).

Only one branch of cofactors, that is the one associated to the D1 protein, is believed to be active in charge separation in PSII, as is also observed in purple bacteria (Trebst 1986). However recent studies suggest the participation of the D2 branch in ET in closed RCs, with Q_A singly reduced and in high light conditions. In this case a photoprotection mechanism involving the participation of the Car of the D2 branch (Car_{D2}) is activated (Martinez-Junza *et al.* 2008). In addition to the four inner Chls discussed above, the isolated D1D2 PSII complex contains two additional loosely coupled peripheral chlorophylls that are not found in bacterial RC (Xiong *et al.* 1998). These Chl's are most probably bound to the exterior of the PSII RC by histidine residues of D1 and D2.

Figure 1.5 A depicts the electron transfer steps occurring inside the PSII RC and the midpoint redox potentials of the involved centers. In PSII systems containing the Q_A secondary electron acceptor, charge separation in the $P_{D1}^{+}Phe_{D1}^{-}$ radical pair is stabilized by the formation of $P_{D1}^{+}Q_A^{-}$. The lifetime of the $P_{D1}^{+}Phe_{D1}^{-}$ radical pair is strongly influenced by the redox state of Q_A ranging from 20 to 250 ns when Q_A is either in the Q_A^{-}

or Q_AH_2 state, respectively, while the P680 triplet (^{3}P680) lifetime increases from 2 µs to 1 ms (van Mieghem *et al.* 1995). From Q_A the electrons are transferred to the more loosely associated quinone Q_B. After taking up two electrons and two protons, Q_B dissociates from the RC as Q_BH_2 and is replaced by a quinone from the surrounding quinone pool. Q_BH_2 delivers the electrons to the cytochrome complex cyt. b_{6f} (Stroebel *et al.* 2003). Through the lumenal space the electrons are subsequently transferred to PSI by the small water-soluble protein named plastocyanin (PC) (Xue *et al.* 1998). In parallel the protons are released to the lumen space, establishing a proton gradient that drives the synthesis of ATP. Upon isolation of the smallest photochemically active PSII complex, namely the ~34kDa D1D2 complex containing only the D1 and D2 proteins, the inner Chl and Phe cofactors remain bound but the OEC as well as Q_B and Q_A are lost (Madjet *et al.* 2009) and ET past the Phe_{D1} acceptor is blocked. This causes a long donor triplet state, as is also observed upon double reduction of Q_A by chemical treatment (Hillmann *et al.* 1995; van Mieghem *et al.* 1995).

1.1.4.2 The electronic structure of the PSII electron donor

The electronic coupling between the two inner chlorophylls P_{D1} and P_{D2} in PSII is much less than for the primary electron donor in the bacterial RC that is also known as the special pair. While the average coupling between the bacterial special pair and the other cofactors is 100 cm^{-1}, the electronic coupling between P_M and P_L is in the range of 500 to 1000 cm^{-1} due to an almost perfect overlap of ring I of P_L with ring I of P_M (Woodbury and Allen 1995). Because of their strong coupling both BChls carry electron spin density (with 68 ± 4 % of the electron density being located on P_L (Daviso 2008)). In contrast, P_{D1} and P_{D2} show a different geometry with P_{D2} being rotated in the plane of the ring I with respect to P_{D1}, causing a dramatic decrease in overlap (Madjet *et al.* 2009; Umena *et al.* 2011). The maximum electronic coupling between P_{D1} and P_{D2} is therefore estimated between 85 cm^{-1} and 150 cm^{-1} (Tetenkin *et al.* 1989; Braun *et al.* 1990; van Kan *et al.* 1990). This renders the inner chlorophyll pair far less ‘special’ among the other cofactors than for the special pair in the bacterial RC, based on their electronic coupling. The individual couplings of P_{D1} and P_{D2} with the accessory Chls and Phe’s are in the range of 50 cm^{-1} (Cardona *et al.* 2012). Whether the PSII donor should be considered monomeric, dimeric or even multimeric, including all six central pigments, is still under discussion. It is

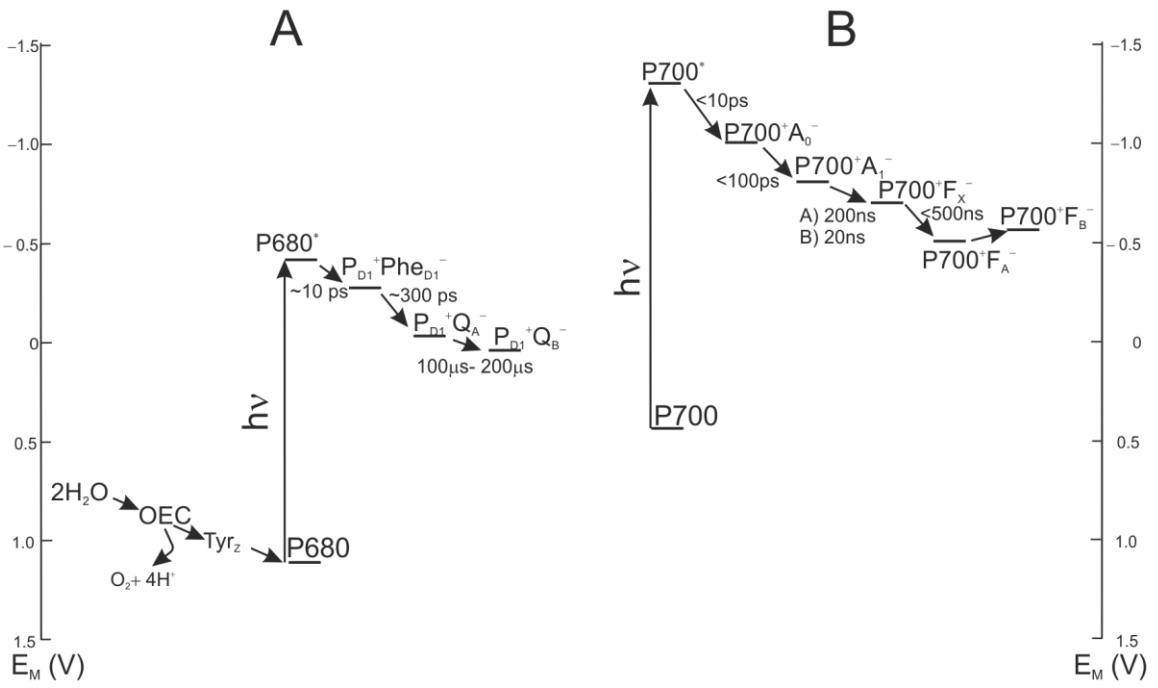

Figure 1.5: Midpoint redox potentials of the components involved in linear electron transfer in PSII (A) and PSI (B) with the rates of forward electron transfer (schematic). Adapted from (Cardona *et al.* 2012; Muh *et al.* 2012, Golbeck 2004). (A) The capacity to generate a potential up to +1.2V (van Gorkom and Schelvis 1993) renders the P680 in PSII capable to extract an electron from a neighboring tyrosine residue. This Tyr_Z amino acid side chain in PSII functions as a bridge between the OEC and P680. The highly reactive tyrosine radical, which is formed upon reduction of $P680^{\bullet+}$, is capable of fully oxidizing the OEC. After 4 successive oxidation steps and the release of 4 protons, two water molecules are split and one oxygen molecule is released by the active site of the OEC (Gorkom and Schelvis 1993; Najafpour and Govindjee 2011). (B) Midpoint redox potentials of centers involved in linear electron transfer in PSI with the rates of forward electron transfer. After excitation of the heterodimer P700, fast ET to the Chl *a* acceptor (A_0) occurs. From A_0 the charge separation is further stabilized by ET to the quinone acceptor A_1 and the three iron-sulphur, [4Fe-3S], clusters F_X, F_A, F_B that function as terminal intrinsic electron acceptors. Adapted from Golbeck 2004.

becoming generally accepted that $P_{D1}P_{D2}$ forms a loosely coupled pair, for which the coupling is unique, both in character and in strength, among the other interactions between the pigments of PSII (Durrant *et al.* 1995; Barter and Klug 2005; Raszewski *et al.* 2008). In this work $P_{D1}P_{D2}$ will be denoted as P680. Due to differences in the direct environment of the two Chl's, most of the dimer HOMO is located on P_{D1} (Nilsson Lill 2011). The cationic state is predominantly located on the P_{D1}, with a $P_{D1}^{\bullet+}/P_{D2}^{\bullet+}$ ratio of ~80:20 (Rigby *et al.* 1994; Diner *et al.* 2001). One reason for this strong asymmetry is the recent finding that if a one electron oxidation is considered, the redox potential of P_{D1} is lower than for P_{D2}, thus favoring the location of the cationic charge on P_{D1} (Saito *et al.* 2012).

PSII can generate a potential up to +1.2V (Gorkom and Schelvis 1993) which is much higher than the potential of 0.5V observed for the special pair electron donor P840 of bacterial photosynthetic RCs (Lin *et al.* 1994). This makes the oxidized electron donor

of PSII, $P680^{\bullet+}$, the strongest oxidizing agent known in nature. Factors that contribute to the high redox potential include;

- differences in the intrinsic electronic and structural properties between Chl *a* and BChl *a* leading to an +160 mV increase (Fajer *et al.* 1975),
- the cation being mainly located on P_{D1} generating a higher charge localization (+140 mV) (Takahashi *et al.* 2008) and asymmetry in the electron spin density (ρ_i) distribution (Diller *et al.* 2005),
- several electrostatic effects with, according to calculations, the highest increase resulting from;
    I. the close proximity of the OEC,
    II. the accumulated effect of the dipoles from the protein backbone and
    III. the atomic charges on the peripheral proteins surrounding the D1/D2 proteins (Ishikita *et al.* 2006).

In addition theoretical calculations suggest an increase (-135 mV) in the oxidative power of P680 due to the amino acid side chains surrounding P_{D1} (Ishikita *et al.* 2006). Previous photo-CIDNP studies on isolated D1D2 particles of spinach suggested a hinge model of the PSII donor involving the axial histidine, His-198, to explain the stabilization of the HOMO on P_{D1} and subsequent increase in the redox potential (Diller *et al.* 2007).

To summarise, the stronger oxidising nature of the cation of PSII opposed to the bacterial RC cation, is in addition to the molecular differences between Chl *a* and BChl *a*, in part due to structural differences, with PSII providing a chlorophyll monomer in a large multiprotein complex that is in the right position to experience a large effect from the backbone dipoles from the trans-membrane helices. This inference fits to the idea that PSII has evolved from a large homodimeric chlorophyll containing a Type I reaction centre ancestor, rather than from the small purple bacterial-type reaction centre (Rutherford and Nitschke 1996, Rutherford and Faller 2003).

Due to the strong overlap of the absorption spectra of the six central pigments in the PSII RC (P_{D1}, P_{D2}, Chl_{D1} and Chl_{D2}, Phe_{D1} and Phe_{D2}), the excitation energy is initially not localized on a single cofactor (Raszewski *et al.* 2008; Shibata *et al.* 2013). Transient absorption experiments on isolated PSII preparations from spinach indicated the existence of two different pathways for ultrafast charge separation with either the P680 or the

accessory Chl_{D1} pigment acting as the primary electron donor at 77 K (Romero *et al.* 2010 and 2012). The latter option results in the formation of the charge separated state $Chl_{D1}^{+}Phe_{D1}^{-}$ prior to the more stable $P680^{+}Phe_{D1}^{-}$ radical pair. In these first picosecond after light absorption even the $P_{D1}^{+}P_{D2}^{-}$ radical pair can occur (Novoderezhkin *et al.* 2011). In contrast to the highly delocalized excited state, the triplet appears to be highly localized on a single Chl (Saito *et al.* 2011). At low temperatures this is the accessory Chl_{D1}, while at higher temperatures, towards physiological conditions, the location of the triplet alternates between Chl_{D1} and P_{D1} (van Mieghem *et al.* 1991; Raszewski *et al.* 2005).

Recently it has been suggested by Acharya *et al.* that isolating the D1D2 complex from its natural environment, (*i.e.* the PSII core complex and surrounding thylakoid membrane), could destabilize the PSII RC and affect the electronic structure of the P680 donor (Acharya *et al.* 2012). Indeed the PSII RC is known to be considerably more fragile upon isolation and interrogation procedures in comparison to PSI and the bacterial RC (Seibert 1993; Cox *et al.* 2010). Detergents commonly used in D1D2 preparations, such as Triton X-100, appear to affect the electron transfer from the Chl_{D1} to the Phe_{D1} acceptor (Tang *et al.* 1991). In addition it was suggested that isolation of the D1D2 PSII RC affects the P680 donor (Hillmann and Schlodder 1995; Riley *et al.* 2004) and leads to a weakening of the coupling between the P_{D1} and P_{D2} cofactors (Acharya *et al.* 2012). These findings question if the isolated D1D2 complex could be used as a proper model for the PSII RC in intact systems.

1.1.5 Photosystem I

In the process of oxygenic photosynthesis electrons flow from PSII to PSI, while the nomenclature follows the order in which the photosystems have been discovered (Emerson and Chalmers 1958; Govindjee and Rabinowitch 1960). The X-ray structure of PSI has been solved in the prokaryotic system of cyanobacteria *Thermosynechococcus elongatus* with 2.5 Å resolution as a trimeric supercomplex, which is depicted in Figure 1.6A (Jordan *et al.* 2001). In the eucaryotic plant system of *Pisum sativum* (Pea) the PSI-LHCI complex has been resolved up to 3.4 Å resolution (Ben-Shem *et al.* 2003). The cyanobacterial PSI core complex consists of 12 subunits containing a total of 96 chlorophylls, while the corresponding plant complex consists of at least 17 subunits harboring over 170 Chls. In cyanobacteria the PSI is mostly observed as a trimer of

monomeric PSI cores (Kruip *et al.* 1994; Fromme *et al.* 2001) while PSI in plants, red algae and green algae is monomeric (Scheller *et al.* 2001; Jensen *et al.* 2003; Kouril *et al.* 2005). Two functional moieties can be distinguished in the PSI supercomplex: the photosystem I core, including the redox active cofactors, and the peripheral light-harvesting complex (LHCI), which serves to increase the light absorption capacity (Schmid *et al.* 1997; Amunts *et al.* 2010). While the structural organization of the redox centers is virtually identical in the structures obtained from Pea and *Thermosynechococcus elongates* (Jordan *et al.* 2001; Amunts *et al.* 2007), the LHCI complex shows a high degree of variability in size, subunit composition and bound pigments. This variation allows each organism to adjust to its specific natural habitat (Boekema *et al.* 2001; Croce *et al.* 2007; Wientjes *et al.* 2009). The PSI core complex is sometimes also denoted as PSI-110 particle referring roughly to the total number (~110) of bound Chls (Mullet *et al.* 1980), and has a molecular weight of ~300 kDa.

1.1.5.1 The Photosystem I reaction center

Figure 1.6B shows the arrangement of the cofactors inside the PSI RC. As in PSII and the bacterial RC, the cofactors in PSI are symmetrically arranged in two parallel chains relative to a pseudo-C_2 symmetry axis perpendicular to the membrane plane in which PSI is embedded in *vivo.* Like Type I bacterial RCs, PSI consists of six chlorophyll molecules, two quinones, and three iron-sulphur [4Fe-3S] clusters (F_X, F_A, F_B), which function as terminal intrinsic electron acceptors. The F_A and F_B clusters operate in series, and are bound by the PsaC subunit. The F_X cluster is located at the interface of the PsaA/PsaB subunits, while the accessory Chls (A_{-1A} and A_{-1B}), the Chl acceptors (A_{0A} and A_{0B}), and the quinone acceptors (A_{1A} and A_{1B}) are bound to either the PsaA (A-branch) or PsaB (B-branch). In comparison to their PSII quinone counterparts, A_{1A} and A_{1B} in PSI are more tightly associated with the protein backbone and not as readily accessible for chemical reducing agents (Srinivasan *et al.* 2009). With distances ranging between 15 and 40 Å, the cofactors in the PSI RC are relatively isolated from the surrounding antenna pigments compared to their PSII and bacterial RC counterparts. The core antenna consists of ~100 tightly packed Chls and 20 β-carotene molecules (Fromme *et al.* 2001).

In addition, the PSI RC contains the heterodimer P700 that consists of one Chl *a* (P_B) and one Chl *a′* (P_A), which is the 13^2-epimer of Chl *a*. Similar to the F_X cluster, P700

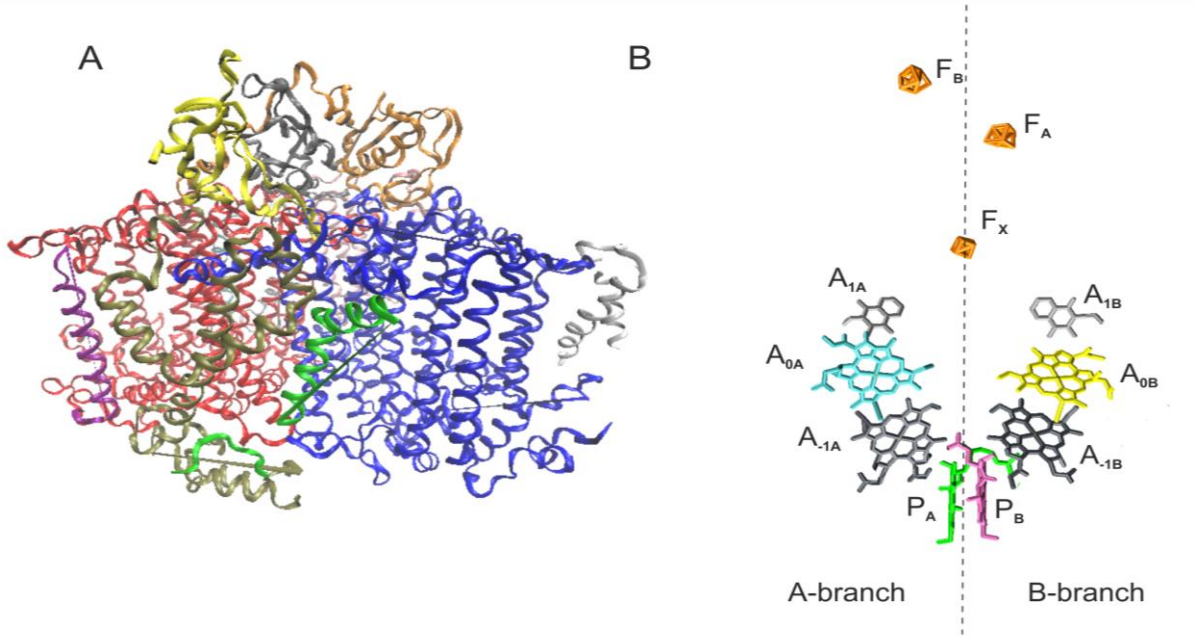

Figure 1.6: (A) The complex arrangement of the trimeric PSI supercomplex with the polypeptide subunits represented in different colors with a ribbon representation. (B) The arrangement of cofactors in the PSI RC. Depicted in pink and green are the two central Chls, P_B and P_A of the Chl *a*/Chl *a'* dimer. In addition the RC contains two accessory Chl *a* (A_{-1A} and A_{-1B}), two donor Chl *a* (A_{0B} and A_{0A}), and two tightly associated phylloquinone's (A_{1A} and A_{1B}). Finally there are three iron-sulphur [4Fe-3S] clusters (F_X, F_A, F_B) which function as terminal intrinsic electron acceptors. Both the A and B branch participate in electron transfer with the relative activity depending mainly on the organism and the reduction conditions. [PDB entry 2WSC (Jordan *et al.* 2001).

is located at the interface of the two branches. While the P_A forms hydrogen bonds to its protein environment, no hydrogen bonds are found on the P_B side (Watanabe *et al.* 1985). The ratio of the spin-density distribution over the P_A/P_B dimer shows strong differences among different species and conditions (Webber and Lubitz 2001): Fourier transform infrared spectroscopy and EPR studies on PSI from *Synechocystis* sp. PCC 6803 cyanobacteria indicated a ratio in the range of 50:50 - 33:67 in favor of the P_B (Breton *et al.* 1999). On the other hand, in spinach and *Thermosynechococcus elongatus* (*T. elongatus*) ratios in the range of respectively 25:75–20:80 and 15:85 have been estimated (Davis *et al.* 1993; Käss *et al.* 2001). Recent theoretical calculations suggested a ratio of 27.9:72.1 based on the coordinates taken from the high resolution X-ray data of *T. elongatus* (Saito and Ishikita 2011). The hydrogen bond of the P_A Chl, the asymmetry in molecular geometry (Chl *a*/Chl *a'*) and minor differences in the protein environment were indicated to be the strongest influences on the relative spin density distribution over P_A and P_B. While P680 in PSII is the strongest oxidizing agent known in nature, P700 is optimized to provide a strong reducing potential. With a potential of approximately -1.2 V,

$P700^{\bullet+}$ is probably the most reducing compound found in natural systems (Ishikita *et al.* 2006).

1.1.5.2 Functional heterogeneity of the Photosystem I RC

Over the past decade intensive investigations of the electron transfer reactions have revealed some unique characteristics of PSI. After the initial suggestions made in 1993 and 1995 by Brettel, Golbeck, Setif and co-workers (Setif and Brettel 1993; Brettel and Golbeck 1995), evidence has been accumulated that, whereas in PSII and bacterial RC the ET proceeds down only one of the cofactor branches, in PSI both branches participate in ET. This process is generally referred to as a 'bidirectional ET' (see for review; (Santabarbara *et al.* 2010)).

Figure 1.5 B (see page 24) depicts the electron transfer steps that occur during linear ET in the PSI RC, and the midpoint redox potentials of the involved centers. Initially it was thought that the electron arriving in PSI was absorbed by the P700 donor, but recent kinetic studies by flash absorption-spectroscopy have questioned if P700 can be rightfully appointed as the primary donor (Holzwarth *et al.* 2006; Müller *et al.* 2010). These studies indicated the accessory chlorophyll A_{-1} as the primary electron donor, resulting in the formation of the radical pair $A_{-1}^{\bullet+}A_0^{\bullet-}$ (with a lifetime of <18 ps) prior to the formation of $P700^{\bullet+}$ $A_0^{\bullet-}$. The identification of the accessory Chl A_{-1} as the primary electron donor in PSI discarded the structural asymmetry of the P700 Chl *a*/Chl *a*' heterodimer as a valid argument against the participation of both branches in ET. A possible explanation for the presence of bidirectional ET in PSI could be the function of the PSI phylloquinone A_1: In Type II RCs (*e.g.* PSII and bacterial RC) the Q_A functions as a 'two electron gate', with a mobile quinone on the inactive branch (Q_B) being used as a terminal acceptor (Müh *et al.* 2012). The quinones present in PSI on the other hand function as single electron carriers facilitating electron transfer to the F_X iron-sulfur cluster. The fact that the quinones of the two branches in PSI function independent of each other, and serve only as intermediates in electron transfer, supports the feasibility of bidirectional ET.

In data obtained from transient optical studies (Holzwarth *et al.* 2006; Müller *et al.* 2010), but also by transient EPR studies (Guergova-Kuras *et al.* 2001), a biphasic forward electron transfers from P700 to A_1 and from A_1 to F_X has been observed. The biphasic

kinetics indicated the presence of two different lifetimes of ~250 and ~20 ns that have been assigned to the oxidation of the quinones A_{1A} and A_{1B}, respectively. The latter was concluded based on site-directed mutagenesis studies showing an increase in the 'slow' 250 ns phase by mutations of residues involved in the coordination of A_{1A}, whereas mutations near A_{1B} influenced the 20 ns phase (Brettel 1997; Joliot and Joliot 1999). Mutations targeting the axial ligands of the A_0 Chl acceptors further confirmed the assignment of the 'fast' phase to the B branch (Guergova-Kuras *et al.* 2001).

The relative activity of the two branches is usually in favor of the A-branch, but seems to vary strongly among different organisms ranging from ~3:2 in green algae (Holzwarth *et al.* 2006; Li *et al.* 2006) to ~3-4 : 1 in cyanobacteria (Ramesh *et al.* 2004; Dashdorj *et al.* 2005). The nature of the strong asymmetry regarding the electron transfer rates to F_X via A_{1A} or A_{1B}, with ET from A_{1B} to F_X occurring 10 times faster than the corresponding ET step on the dominant A branch, is still under discussion. A possible explanation could be the differences in the orientation of A_{1A} and A_{1B} in their respective protein pockets, facilitating a strong H-bond between the A_{1A} cofactor and the protein backbone, which is absent on the A_{1B} side (Berthold *et al.* 2012). Another explanation is the effect of the relative redox potentials of the A and B side phylloquinones on the transfer rate as is described by Marcus theory (Ptushenko *et al.* 2008). Past the phylloquinones cofactors the two branches merge in the F_X cluster from where electrons are passed via the F_A and F_B clusters to ferredoxin in 500 ns, driving ultimately the formation of NADPH by Ferredoxin-NADP reductase (FNR, see Figure 1.1 on page 14).

While consensus on the bidirectional nature of ET in both prokaryotic and eukaryotic PSI has been reached (Fairclough *et al.* 2003; Cohen *et al.* 2004; Redding *et al.* 2007), the molecular details of the mechanism have not yet been elucidated (Berthold *et al.* 2012). Since the first observations of the biphasic nature of the A_1^- oxidation were obtained from isolated PSI particles (Setif and Brettel 1993; Brettel and Golbeck 1995), the presence of the 'fast' lifetime was initially suggested to result from purification artifacts. Although the conservation of the biphasic nature in whole cells of green algae (Joliot and Joliot 1999) ruled out this possibility, the isolation level and subsequent presence of detergents did seem to influence the relative branch activity (Brettel and Golbeck 1995). In addition the oxidation state of the quinones seems to affect the relative branch activity with *e.g.* ET in *Synechococcus lividus* occurring solemnly along the B branch at low temperature (100K) and strong reducing conditions (Poluektov *et al.* 2005).

Thus the mechanistic nature of bidirectional electron transfer in PSI across different species and sample preparation remains unresolved.

1.2 PHOTO-CIDNP

1.2.1 The Solid State Photo-CIDNP effect

Nuclear spin hyperpolarization, *i.e*. the creation of large, non-equilibrium population differences between nuclear spin states, allows for a significant enhancement of signal intensities in NMR experiments. This signal increase is crucial for NMR investigations where sensitivity represents a limiting factor, such as the characterization of large (bio)molecular systems as photosystems. Similar to other hyperpolarization methods, including spin-exchange optical pumping and dynamic nuclear polarization (DNP), photochemically induced dynamic nuclear polarization (photo-CIDNP) realizes this process via a polarization transfer from electron spins to nuclear spins.

Photo-CIDNP is a well-known phenomenon in liquid NMR. In the liquid state it was discovered in 1967 and explained by the radical pair mechanism (RPM) (for review see: Bargon and Fischer 1967; Ward and Lawler 1967; Cocivera 1968; Closs and Closs 1969; Kaptein and Oosterhoff 1969; Hore and Broadhurst 1993; Roth 1996; Goez 1997). In 1994, Zysmilich and McDermott observed the photo-CIDNP effects in solids for the first time in frozen and quinone-blocked RCs of purple bacteria of *Rb. sphaeroides* R26 by ^{15}N magic-angle spinning NMR (Zysmilich and McDermott 1994). Since the RPM depends also on diffusion, it could not provide the complete explanation for the solid-state photo-CIDNP. Meanwhile much progress has been made in resolving the spin-chemical mechanisms of the solid-state photo-CIDNP effect (for reviews see: (Jeschke and Matysik 2003; Roy *et al.* 2007), and in particular for RCs of *Rb. sphaeroides* it is now well understood and will be discussed in more detail in section 1.2.2 (Daviso *et al.* 2009).

Up to this point the solid-state photo-CIDNP effect has been observed in a wide variety of photosynthetic RCs; purple bacteria *Rb. sphaeroides* WT (Prakash *et al.* 2005), its Car lacking mutant R26 (Prakash *et al.* 2006), *Rhodopseudomonas acidophila* (Diller *et al.* 2008), *Heliobacillus mobilis* (Roy *et al.* 2008; Thamarath *et al.* 2012), green sulfur bacteria *Chlorobium tepidum* (Roy *et al.* 2007), and isolated higher plant photosystems I and II from *Spinacias oleracea* (Matysik 2000; Alia *et al.* 2004; Diller *et al.* 2007; Diller *et al.* 2007). The detection of the effect across a range of otherwise rather different

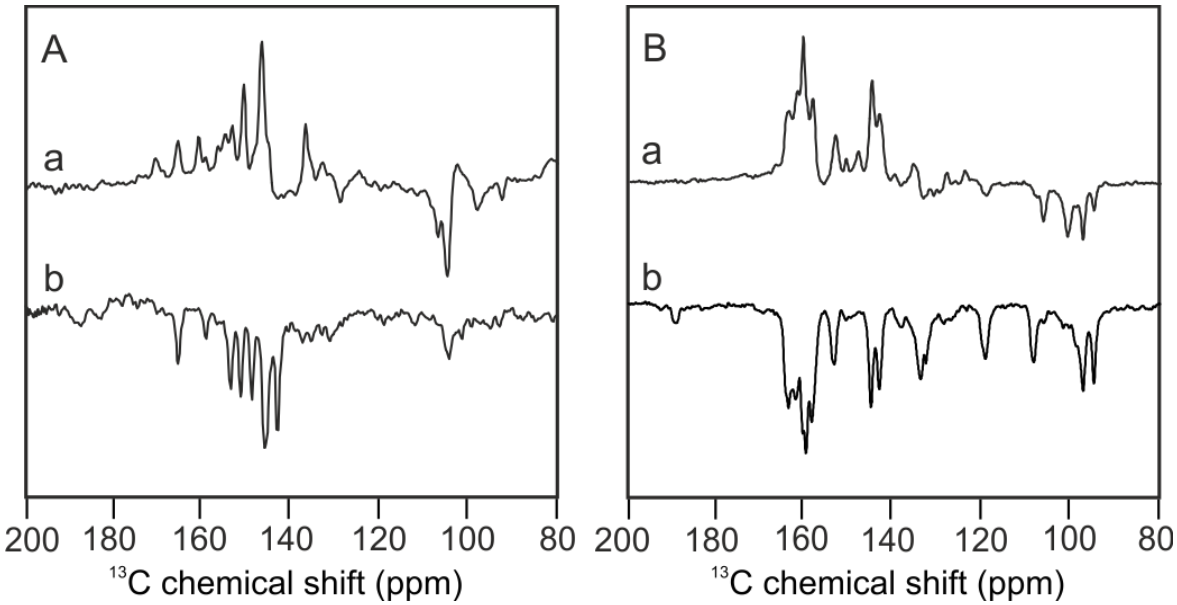

Figure 1.7: ^{13}C photo-CIDNP MAS NMR spectra collected from (A) isolated D1D2 (a) and PSI-110 (b) from spinach and (B) RCs of *Rb. sphaeroides* R26 (a) and WT (b). The data were obtained by continuous illumination with white light at 223 K. The sign pattern of the photo-CIDNP spectrum obtained from PSII (A,a) is similar to the sign pattern observed for the R26 mutant (B,a), due to the relatively long triplet lifetimes (~1ms and 100 µs, respectively, opposed to 10 µs in *Rb. sphaeroides* WT). The similarity between the sign patterns observed in PSI and *Rb. sphaeroides* WT is less straightforward and will be further discussed in Chapter 5.

photosynthetic RCs suggests that the occurrence of photo-CIDNP is related to an optimization of the first ET step and may thus be a guide for the improvement of artificial systems.

Photo-CIDNP has been observed for intact bacterial RC-LH core complexes embedded in the chromatophore membrane of selectively ^{13}C isotope labeled whole cells of purple bacteria (Prakash *et al.* 2003). Addition of detergent, causing dissociation of the bacterial RC-LH complexes from the membrane, resulted in a dramatic decrease in the intensity of the light induced signals. The pronounced differences between intact membrane-bound and detergent solubilized bacterial RC-LH complexes were tentatively explained by the loss of self-orientation upon solubilization. Photo-CIDNP MAS NMR studies of whole cells of heliobacteria (*Heliobacillus mobilis*) (Thamarath *et al.* 2012) indicated the occurrence of symmetric electron transfer via both branches of cofactors in this organism.

^{13}C-Photo-CIDNP experiments on PSII and PSI were restricted to isolated PSII D1D2 and PSI-110 complexes due to the difficulty to incorporate selective labels in plants. Previous experiments on isolated natural abundance samples of PSII and PSI

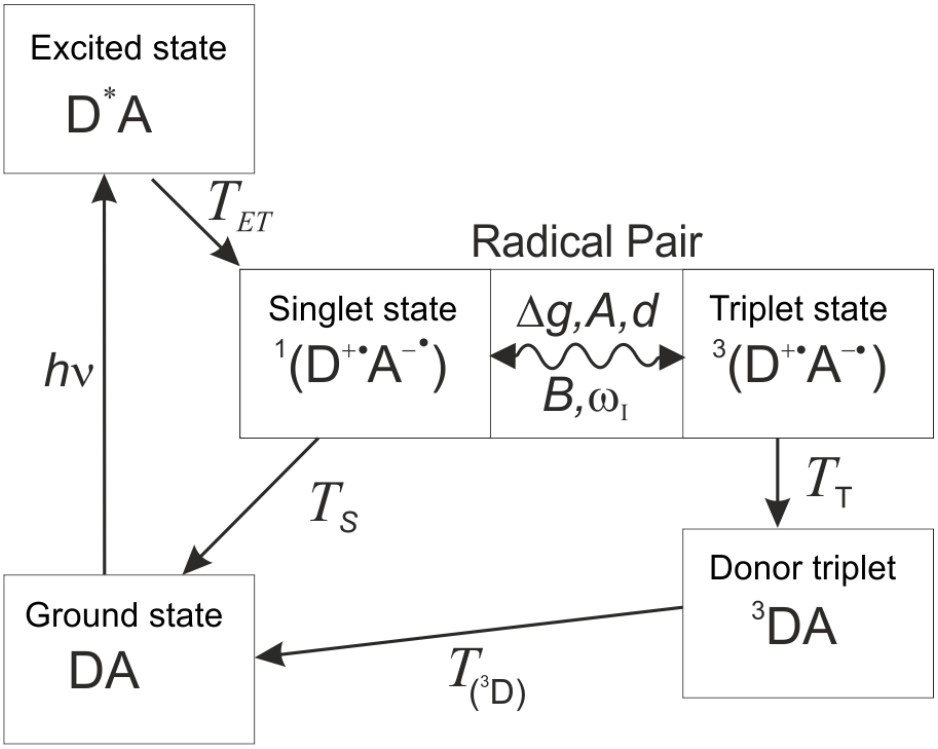

Figure 1.8: Schematic representation of the photocycle in photosynthetic RCs. After absorption of a photon, electron transfer occurs from the donor (D), (*e.g.* P_MP_L in purple bacteria, P_{D1} in PSII or P_B in PSI), to the primary acceptor (A), (*e.g.* Φ_L in purple bacteria, Phe_{D1} in PSII and A_0 in PSI). The initial excited state D*A is followed by electron transfer to form the correlated radical pair in its non-stationary singlet state. The radical pair can decay via its singlet state $^1(D^{+\bullet}A^{-\bullet})$ or convert its electronic zero quantum coherence into double quantum coherence in the triplet state $^3(D^{+\bullet}A^{-\bullet})$ by coherent electron-nuclear spin evolution. This TSM process depends on the difference of the *g* value between the two electrons, Δg, the secular part of the hyperfine interaction, *A*, the coupling between the two electrons, *d*, the pseudo-secular hyperfine coupling, *B*, and the nuclear Zeeman frequency, ω_I. The triplet state can decay back to the ground state via the triplet donor state, ^{3}DA.

rendered spectra with different sign patterns (Figure 1.7). Spectra obtained from isolated PSI showed only emissive signals, as has also been observed in spectra obtained from *Rb. sphaeroides* WT. Isolated PSII D1D2 on the other hand provided a spectrum with both emissive and absorptive signals in a pattern similar to those observed from the R26 mutant of *Rb sphaeroides*. This similarity is in line with a long distance (20 Å) of the P_{D1} donor to the Car in PSII and correspondingly slow triplet quenching for the P_{D1} donor (Matysik 2000; Diller *et al.* 2005). The signal doubling observed in spectra obtained from *Rb sphaeroides*, indicating a dimeric donor, is absent for both PSII and PSI.

1.2.2 The Mechanism of Solid State Photo-CIDNP

Based on experimental data from *Rb. sphaeroides* and corresponding computational work, the mechanism of photo-CIDNP in bacteria has been well established

(Daviso *et al.* 2009). Figure 1.8 depicts the photocycle occurring in photosynthetic RCs and the radical pairs produced upon illumination are shown. Initially, the spin-correlated radical pair is formed in a pure singlet state and and has, therefore, a high electron spin order. Three different mechanisms, which run in parallel, build up photo-CIDNP under continuous illumination; electron-electron-nuclear three-spin mixing (TSM), differential decay (DD) and differential relaxation (DR).

Electron-electron-nuclear three-spin mixing (TSM) breaks the antisymmetry of the population of the nuclear states by coherent spin evolution in the correlated radical pair and depends on the signs of the electron-electron and of the electron nuclear interactions (Jeschke 1997; 1998). The symmetry breaking is driven by the off-diagonal, pseudosecular, part of the hyperfine interaction. The contribution of TSM through spin mixing is maximized when the difference of the electron Zeeman frequencies ($\Delta\Omega$), the nuclear Zeeman frequency (ω_I), and the secular part of the hyperfine interaction (A) match. This is reflected in the double matching condition: $2|\Delta\Omega| = 2|\omega_I| = 2|A|$.

In the differential decay (DD) mechanism (Polenova and McDermott 1999), the symmetry between the two decay channels is broken by the different lifetimes of the singlet and triplet state and by the pseudosecular part of the hyperfine interaction. The result is an additional imbalance between the fractions of nuclei in spin-up and spin-down states in the two decay channels. To maximize the symmetry breaking caused by the DD mechanism only a single matching of interactions, that is $2|\omega_I| = 2|A|$, is required and the difference of the singlet and triplet radical pair lifetimes should be of the order of the inverse hyperfine coupling.

In samples of RCs with a long lifetime of the triplet donor (^{3}P), such as in RCs of the R26 mutant of *Rb. sphaeroides* which lack the carotenoid, a third mechanism creating nuclear polarization may occur in addition to the two polarization transfer mechanisms TSM and DD. In this differential relaxation (DR) mechanism, which is called 'Cyclic reactions' in the liquid-CIDNP language, the breaking of antisymmetry of the polarization in the singlet and triplet branches occurs in a non-coherent way. The enhanced relaxation of nuclear spins in the proximity of the high-spin donor partially cancels the nuclear polarization in the donor cofactor. Hence, when the ^{3}P lifetime is comparable to or exceeds the paramagnetically enhanced longitudinal relaxation time, net polarization occurs due to partial extinction of nuclear polarization of the triplet state of the radical pair (Goldstein and Boxer 1987; McDermott *et al.* 1998). A strong contribution of the DR mechanism is also observed in PSII (spectrum 1.7Aa, page 30) where the long distance

between the Car and P680 causes a long-lived triplet (^{3}P680) and subsequent buildup of nuclear polarization by DR. The similarity of the signal pattern of the spectrum obtained from PSI (spectrum 1.7Ab) to that obtained from WT *Rb. sphaeroides* (spectrum 1.7Bb) suggests the absence of DR contribution in these samples.

1.3 SCOPE OF THIS THESIS

In this thesis the advantages of photo-CIDNP MAS NMR in combination with isotope labeling are demonstrated. The main aim is to show how the combination of photo-CIDNP signal enhancement with the increased selectivity and sensitivity obtained by isotope labeling, can be applied to study the electronic structure of the electron donor in PSI and PSII RCs with atomic resolution, even directly in intact systems. In this way pending questions can be addressed regarding: 1) The conservation of the photo-CIDNP effect in whole cells of cyanobacteria. 2) The conservation of the electronic ground state of the PSI electron donor and its functional heterogeneity in different plant species and under different sample conditions. 3) The conservation of the electronic structure of the P_{D1} electron donor upon PSII isolation. In addition to the obtained refinements in the photo-CIDNP signal assignments and the application of time-resolved photo-CIDNP to plant systems, a model for the mechanism of photo-CIDNP buildup in intact PSII systems that contain the OEC is constructed and the mechanism of photo-CIDNP buildup in PSI is discussed (Chapter 4).

Photo-CIDNP has been observed for selectively ^{13}C isotope labeled whole cells of purple- and heliobacteria (Prakash *et al.* 2003; Thamarath *et al.* 2012), while previous attempts to selectively label plants failed, limiting photo-CIDNP studies of PSII and PSI to the fully isolated systems, namely PSII D1D2 complexes and PSI-110 particles (Matysik 2000; Alia *et al.* 2004; Diller *et al.* 2005).

In **chapter 2** photo-CIDNP ^{13}C MAS NMR data of PSI obtained directly from selective ^{13}C- isotope labeled whole cells of cyanobacteria *Synechocystis* sp. PCC 6803 are presented, showing photo-CIDNP signals from cyanobacterial PSI in its natural membrane environment. In the growing list of natural RCs proven to show the solid-state photo-CIDNP effect, RCs of cyanobacteria (blue-green algae) remained to be a blank spot. Cyanobacteria are model microorganisms for the study of plant photosynthesis having a photosynthetic apparatus very similar to the one found in plants while being suitable for mutagenesis studies.

Chapter 3 adresses the question whether variations associated with different organisms affect P700 with its highly optimized redox properties. Data obtained from ^{15}N-labeled PSI-110 particles from spinach and duckweed are presented in order to compare these two organisms. The data demonstrate that the ratio of activity of both branches is modified between different species.

In **chapter 4** data of selectively ^{13}C labeled duckweed at different stages of isolation are presented, all the way from isolated D1D2 particles to entire plants. The main question addressed in this chapter is whether the electronic structure of the non-stationary correlated radical pair state observed in the isolated D1D2 complex is different compared to the electronic structure observed in intact RC in the PSII core in higher preparations. In addition we will compare the electronic structure of the PSII electron donor in spinach and duckweed.

In **chapter 5** the first time-resolved photo-CIDNP data sets obtained from plant photosystems will be presented. It includes a discussion of the results obtained upon applying ns laser flash photo-CIDNP MAS NMR to uniformly ^{15}N and selectively ^{13}C labeled PSI and natural abundance D1D2 PSII complex and compares the experimental data with theoretical calculations.

Chapter 6 provides an outlook on future applications of photo-CIDNP to selectively labeled PSII and PSI. In addition the apparent strong field dependence of PSI photo-CIDNP will be discussed and illustrated by prelimenairy results obtained by ^{13}C photo-CIDNP MAS NMR data obtained from selectively ^{13}C labeled PSI-110 particles of duckweed. Finally it includes the first results obtained from selectively ^{15}N-ALA labeled PSII.